6-28-2006

Semiclassical Nonadiabatic Dynamics Based on Quantum Trajectories for the $O(^3P,^1D)+H_2$ System

Sophya Garashchuk
University of South Carolina--Columbia, sgarashc@chem.sc.edu

Vitaly A. Rassolov
University of South Carolina - Columbia, rassolov@chem.sc.edu

George C. Schatz
Northwestern University

Publication Info

Published in *Journal of Chemical Physics*, Volume 124, Issue 24, 2006, pages 244307-.

Semiclassical nonadiabatic dynamics based on quantum trajectories for the $O(^3P,^1D)+H_2$ system

Sophya Garashchuk[a)]
Department of Chemistry and Biochemistry, University of South Carolina, Columbia, South Carolina 29208 and Department of Chemistry, Northwestern University, Evanston, Illinois 60208-3113

Vitaly A. Rassolov
Department of Chemistry and Biochemistry, University of South Carolina, Columbia, South Carolina 29208

George C. Schatz
Department of Chemistry, Northwestern University, Evanston, Illinois 60208-3113

(Received 11 April 2006; accepted 5 May 2006; published online 28 June 2006)

The $O(^3P,^1D)+H_2 \rightarrow OH+H$ reaction is studied using trajectory dynamics within the approximate quantum potential approach. Calculations of the wave-packet reaction probabilities are performed for four coupled electronic states for total angular momentum $J=0$ using a mixed coordinate/polar representation of the wave function. Semiclassical dynamics is based on a single set of trajectories evolving on an effective potential-energy surface and in the presence of the approximate quantum potential. Population functions associated with each trajectory are computed for each electronic state. The effective surface is a linear combination of the electronic states with the contributions of individual components defined by their time-dependent average populations. The wave-packet reaction probabilities are in good agreement with the quantum-mechanical results. Intersystem crossing is found to have negligible effect on reaction probabilities summed over final electronic states. © *2006 American Institute of Physics*. [DOI: 10.1063/1.2208615]

I. INTRODUCTION

Molecular dynamics is an established theoretical tool for studies of large molecular systems containing hundreds of atoms. Its limitation—classical motion of nuclei on a single electronic potential-energy surface (PES)—is well known, but the cost of exact quantum-mechanical methods, which rises exponentially with system size, limits their applicability to systems of a few atoms. The development of a semiclassical trajectory method that retains the favorable scaling of classical dynamics and incorporates the dominant quantum effects is therefore a long-standing goal.

Arguably, nonadiabatic dynamics is the most important quantum effect on the motion of nuclei in chemical reaction dynamics, being important in reactive scattering, photochemistry, and enzymatic reactions.[1–3] Quantum tunneling becomes negligible for heavy nuclei and quantum interference is often quenched in large molecular systems at short times due to the wave-function decoherence, but nonadiabatic effects can still influence such systems. The most widely used method for including nonadiabatic effects into the dynamics of molecules is the trajectory surface hopping method (TSH),[4,5] which is based on classical evolution of trajectories that can switch between different electronic states. Some recent applications include the photodissociation of ozone,[6] and of formic acid.[7] Maiti and Schatz have used TSH to study spin-orbit interaction induced intersystem crossing effects in the $O+H_2$ reaction, including four PESs in this model.[8] This reactive system has been thoroughly investigated both experimentally and theoretically,[9–12] although the first quantum wave-packet study involving four coupled electronic surfaces has been reported only recently.[13] Accurate PESs are available due to Rogers *et al.*[14] and Dobbyn and Knowles,[15] and the spin-orbit couplings have been determined by Hoffmann and Schatz.[16] In the quasiclassical trajectory surface hopping study[8] it was estimated that intersystem crossing effects enhance total reaction cross sections up to 20%, whereas essentially no such effect was found in the quantum results of Ref. 13.

In this work we combine the recently developed approximate quantum potential (AQP) method in curvilinear Jacobi coordinates[17,18] with a mixed wave-function representation[19,20] to give an efficient semiclassical description of the leading quantum mechanical (QM) effects of the single surface dynamics and of the nonadiabatic effects for $O(^3P,^1D)+H_2$. The relation between our treatment of nonadiabatic dynamics and the trajectory surface hopping method is discussed in Sec. II B.

The AQP approach is based on an approximate determination of the quantum potential

$$U = -\frac{\hbar^2}{2m}\frac{\nabla^2 A}{A}$$

arising in the hydrodynamic or Bohmian formulation of the Schrödinger equation (SE),[21] based on the polar representation of the wave function

[a)]Electronic mail: sgarashc@mail.chem.sc.edu

$$\phi(\mathbf{x},t) = A(\mathbf{x},t)\exp\left(\frac{i}{\hbar}S(\mathbf{x},t)\right) \tag{1}$$

in terms of its real amplitude $A(\mathbf{x},t)$ and phase $S(\mathbf{x},t)$. The wave-function density,

$$\rho(\mathbf{x},t) = A^2(\mathbf{x},t), \tag{2}$$

satisfies the continuity equation. The phase S is identified with the action function for a trajectory of a particle of mass m evolving under the combined influence of the classical potential V and the quantum potential U. The nonlocal potential U, responsible for all QM effects in the system, is generally singular which makes its exact computation often prohibitively expensive. The AQP approach is semiclassical; it introduces the leading quantum effects into trajectory dynamics and its error vanishes in the $\hbar \to 0$ limit. It has a well-defined classical limit, $U=0$, and can be taken toward the QM limit when sophisticated approximations of U are employed. A global linear approximation to the nonclassical component of the momentum operator,

$$\mathbf{r} = \hbar\frac{\nabla A}{A}, \tag{3}$$

from which an approximate quadratic quantum potential and linear force are obtained analytically, is computationally very cheap. The resulting potential is exact for Gaussian wave packets and can describe tunneling and zero-points energy effects in chemical systems as was shown for two-dimensional H_3 and ICN model systems.[22] This approximation can be improved by linearizing $\mathbf{r}$ on subspaces[23] or by including higher-order basis functions representing $\mathbf{r}$. For example, and exponential function gives the exact description of the Morse oscillator eigenstates.[18] The mixed wave-function representation,

$$\psi(\mathbf{x},t) = \chi(\mathbf{x},t)\phi(\mathbf{x},t),$$

where the polar part $\phi(\mathbf{x},t)$ is represented in terms of quantum trajectories and the coordinate space prefactor $\chi(\mathbf{x},t)$ is computed approximately for each trajectory, gives a cheap description of the nodes in the wave-function density[24] or of the nonadiabatic effects.[19]

Following up our prior work with one-dimensional nonadiabatic models[20] and the implementation of the quantum trajectory method in curvilinear coordinates[18] for the $O+H_2$ system, we use the AQP method to study the reactive dynamics of $O(^3P_{2,1,0},{}^1D)+H_2$ in the ground rovibrational state in three dimensions on four coupled electronic surfaces. Over the last few years a variety of quantum trajectory based methods have been suggested in coordinate space[25–31] and as well as in phase space[32–38] and implemented for a variety of model systems including high-dimensional (up to 100 dimensions) models.[39,40] To the best of our knowledge the current study is the largest quantum trajectory application to a realistic scattering system. The methodology is described in Sec. II. Section III contains details of the implementation, results, and discussion. Section IV concludes. Atomic units are used throughout the paper.

II. NONADIABATIC TRAJECTORY FORMULATION IN JACOBI COORDINATES

The simple form of the kinetic energy in Cartesian coordinates is convenient both for the classical trajectory propagation and for the quantum trajectory formulation. However, experimental and theoretical studies of chemical reactions are often performed for systems prepared in well-defined quantum states using Jacobi-type coordinates that are designed to describe the uncoupled motion of the fragments at large separation. Bond coordinates are often employed in spectroscopic studies. To allow for direct comparison with other theoretical methods that used these different coordinates systems, as well as with experiment, we have generalized the quantum trajectory approach to arbitrary coordinate systems.[18] The formulation for three-dimensional Jacobi coordinates is given below.

A. Dynamics of quantum trajectories

The description of an isolated molecular system generally relies on separation of the motion of the center of mass and overall rotation from internal motion of the constituents. In this case, it is natural to begin with the case of zero total angular momentum, as methods for extending the $J=0$ calculations to higher J are well known. A nonrotating triatomic molecule can be described in the Jacobi coordinates $\mathbf{x}=\{x,y,\theta\}$, where y is the diatomic internuclear separation, x is the distance between the third atom and the center of mass of the diatomic, and θ is the angle between x and y. The SE is usually solved for the wave function divided by xy so that the volume element becomes

$$J\Omega = \sin\theta\delta\theta\delta x\delta y. \tag{4}$$

The quantum-mechanical Hamiltonian, taking into account the Jacobian of the coordinate transformation, is

$$\hat{H} = \hat{T} + V, \tag{5}$$

$$\hat{T} = -\frac{1}{2M}\frac{\partial^2}{\partial x^2} - \frac{1}{2m}\frac{\partial^2}{\partial y^2} - \frac{1}{2\mu}\left(\frac{\partial^2}{\partial\theta^2} + \cot\theta\frac{\partial}{\partial\theta}\right), \tag{6}$$

where the moment of inertia is included using

$$\frac{1}{\mu} = \frac{1}{Mx^2} + \frac{1}{my^2}. \tag{7}$$

The reduced mass of the diatomic, m, is associated with the coordinate y. The reduced mass of the atom + diatomic, M, is associated with the coordinate x. Substitution of the wave function in terms of the real amplitude A and phase S of Eq. (1) into Eq. (5) leads to a time dependence of S that is equivalent to that of the action function of a trajectory evolving according to the classical Hamiltonian,

$$\frac{dS}{dt} = \frac{p_x^2}{2M} + \frac{p_y^2}{2m} + \frac{p_\theta^2}{2\mu} - (V+U). \tag{8}$$

With the following definition of the gradient,

$$\nabla = \left(\frac{\partial}{\partial x}, \frac{\partial}{\partial y}, \frac{\partial}{\partial \theta}\right), \tag{9}$$

the momentum of a trajectory is

$$\mathbf{p} = \nabla S, \tag{10}$$

and its velocity $\mathbf{v}$ is

$$\mathbf{v} = \left(\frac{p_x}{M}, \frac{p_y}{m}, \frac{p_\theta}{\mu}\right). \tag{11}$$

The full time-derivative is

$$\frac{d}{dt} = \frac{\partial}{\partial t} + \mathbf{v}^T \nabla . \tag{12}$$

U is the quantum potential that we find convenient to define in terms of the nonclassical momentum given by Eqs. (3) and (9) as

$$U = -\frac{1}{2}\left[\frac{1}{M}\left(r_x^2 + \frac{\partial r_x}{\partial x}\right) + \frac{1}{m}\left(r_y^2 + \frac{\partial r_y}{\partial y}\right) + \frac{1}{\mu}\left(r_\theta^2 + \frac{\partial r_\theta}{\partial \theta} + r_\theta \cot\theta\right)\right]. \tag{13}$$

Equations of motion of a trajectory that are consistent with Eq. (8) are

$$\frac{d\mathbf{p}}{dt} = -\nabla(V+U), \quad \frac{d\mathbf{x}}{dt} = \mathbf{v}. \tag{14}$$

Formally, the wave-function density given by Eq. (2) evolves according to

$$\frac{d\rho}{dt} = -\left(\frac{1}{M}\frac{\partial p_x}{\partial x} + \frac{1}{m}\frac{\partial p_y}{\partial y} + \frac{1}{\mu}\frac{\partial p_\theta}{\partial \theta} + \frac{\cot\theta}{\mu}p_\theta\right)\rho, \tag{15}$$

but we do not compute it explicitly. Instead of Eq. (15) we use trajectory weights

$$w = \rho J \Omega, \quad \frac{dw}{dt} = 0, \tag{16}$$

based on Eq. (4), which do not change in time for a closed system,[18] to determine expectation values needed for the AQP parameters and for computation of probabilities.

B. Nonadiabatic formulation

Consider dynamics on multiple coupled potential surfaces in the diabatic representation

$$i\frac{\partial}{\partial t}\boldsymbol{\psi} = (\hat{T}\mathbf{I} + \mathbf{V})\boldsymbol{\psi}. \tag{17}$$

Here $\mathbf{I}$ is the identity matrix whose size is given by the number of PESs. The kinetic-energy operator is given by Eq. (5). The matrix $\mathbf{V}$ is a symmetric matrix that contains the diabatic PESs and couplings. Our approach to nonadiabatic dynamics in the framework of quantum trajectories is based on a mixed representation of the wave function as described in Ref. 20. The basic idea is to represent the wave-function components as a product of the polar part describing the overall dynamics in coordinate space and of the coordinate space prefactor describing the amplitude changes due to coupling between the surfaces. In the most general case the ith component of the wave function is

$$\psi_i = \sum_j \chi_{ij}(x,y,\theta,t)\phi_j(x,y,\theta,t),$$

with indexes i,j labeling electronic states. The polar parts $\phi_j(x,y,\theta,t)$ can evolve on the diabatic or nonadiabatic PESs, or on effective potential surfaces. For the OH_2 system the lowest $^3P_{2,1,0}$ and ^1D PESs become degenerate in the product region,[16] which is also the region of nonzero spin-orbit coupling. Therefore, the cheapest formulation of the mixed representation nonadiabatic dynamics involving a single ϕ can be applied, as verified in one-dimensional model studies.[20] The multidimensional version of this formulation is given below. We use the following representation of the wave function:

$$\psi_i(x,y,\theta,t) = \chi_i(x,y,\theta,t)\phi(x,y,\theta,t). \tag{18}$$

The dynamics of ϕ is governed by a so-far unspecified potential, V_d,

$$i\frac{\partial}{\partial t}\phi = (\hat{T} + V_d)\phi. \tag{19}$$

Then, from Eq. (17) the time evolution of the coordinate space prefactor $\boldsymbol{\chi}$ is governed by

$$i\frac{\partial}{\partial t}\boldsymbol{\chi} = -i(\mathbf{v}^T\nabla)\boldsymbol{\chi} + (\hat{T}_c + \hat{T})\mathbf{I}\boldsymbol{\chi} + (\mathbf{V} - V_d\mathbf{I})\boldsymbol{\chi}. \tag{20}$$

The operator $\hat{T}_c$ couples $\mathbf{r}$ with the first derivatives of $\boldsymbol{\chi}$,

$$\hat{T}_c = -\frac{r_x}{M}\frac{\partial}{\partial x} - \frac{r_y}{m}\frac{\partial}{\partial y} - \frac{r_\theta}{\mu}\frac{\partial}{\partial \theta}. \tag{21}$$

Equations (19) and (20) are equivalent to the original SE (17). For an efficient trajectory implementation the evolution of ϕ and χ is determined approximately. Equation (19) is solved using the AQP approach as detailed in Ref. 18. Equation (20) is simplified in the following manner: (i) The first term on the right-hand side (RHS) is combined with the left-hand side (LHS) to give the time derivative of $\boldsymbol{\chi}$ along a trajectory; (ii) the effect of $\hat{T}_c$ and $\hat{T}$ terms, which are small in the limit of large mass, is minimized by the choice of the effective potential V_d. Then, these derivative terms can be neglected or approximated using a small basis set. Typical initial conditions for a wave function—a single (kth) populated electronic state—are $\{\phi = \psi_k, \chi_i = \delta_{ik}\}$. In this case $\boldsymbol{\chi}$ will be smoother if the elements of the potential part in Eq. (20) are small. Minimization of these elements suggests the following form of the effective potential:

$$V_d = \frac{\sum_{ij}\langle\chi_i|\chi_j\rangle V_{ij}}{\sum_i \langle\chi_i|\chi_i\rangle}. \tag{22}$$

Then, the approximate equation for $\boldsymbol{\chi}$ is

$$i\frac{d}{dt}\boldsymbol{\chi} = (\mathbf{V} - V_d\mathbf{I})\boldsymbol{\chi}. \tag{23}$$

The form of the effective potential, Eq. (22), which determines the dynamics of a single set of trajectories, is related to the trajectory dynamics used in the TSH method. If we consider the classical limit of the above approach, i.e., we set the quantum potential to zero, then the trajectories can be propagated independently, once the averaging in Eq. (22) is removed. If we postulate that the populations $|\chi_i|^2$ defining the potential in Eq. (22) are equal to either 0 or 1, while the continuous functions χ_i computed from Eq. (20) define the probabilities of switching between these two values, then the resulting strategy is similar to the trajectory hopping. In TSH the assumption of trajectory propagation on a single diabatic or adiabatic surface guarantees uncoupled dynamics in the asymptotic regions. In our formulation this requirement is fulfilled in the formulation with multiple sets of trajectories.[20]

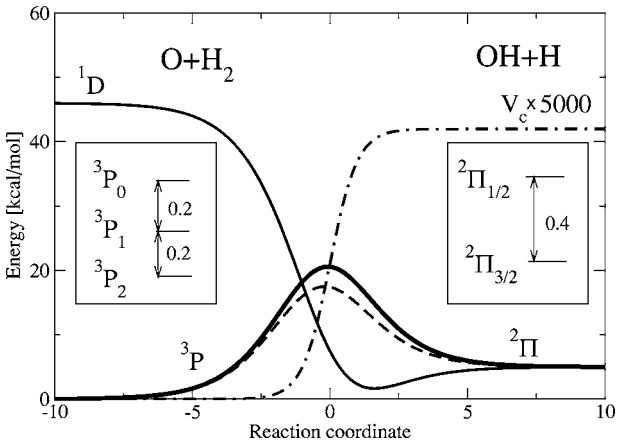

FIG. 1. Diabatic electronic states. $^1A'$ correlates with ^1D state (thin solid line). $^3A''$ correlates with $^3P_2$ and $^3P_1$ states (thick solid line). $^3A'$ correlates with $^3P_0$ state (dashed line). The asymptotic coupling is shown with the dot-dashed line. Asymptotic splittings of the adiabatic PESs are indicated in the insets in kcal/mol.

III. DYNAMICS OF $O(^3P,^1D)+H_2$ IN THREE DIMENSIONS

A. Implementation

The formalism of Sec. II has been applied to the four state model describing the spin-orbit interaction induced intersystem crossing of the $O+H_2 \rightarrow OH+H$ reaction, developed by Hoffmann and Schatz.[16] Spin-orbit interaction in the ground configuration of the oxygen atom results in 15 electronic states: five $^1D_2$, one $^1S_0$, and nine ^3P states. The $^1S_0$ is high in energy and is ignored. Out of the five singlet states correlating to $O(^1D)$ only one state ($^1A'$) crosses the triplet states for energies of interest to this study, so this is one of the four states included in the model. The ^3P states of oxygen have asymptotic degeneracies (5,3,1) corresponding to values of the total angular momentum (2,1,0), respectively. At short range these states correlate to $^3A''$, $^3A''$, and $^3A'$ surfaces. According to the treatment of Hoffmann and Schatz, only three of these nine are included in the four state model as only three have significant spin-orbit couplings with the one singlet state, and also correlate to ground-state products. This occurs because one of the (triply degenerate) $^3A''$ states correlates to excited products ($^2\Sigma$ states of OH) and is, therefore, nonreactive at the energies considered. This reduces the nine states to six. Of the remaining six states there is parity decoupling such that only half of these couple to the singlet surface. Consequently, the (5,3,1) degeneracy for $O(^3P_{2,1,0})$ becomes (1,1,1) in this model. For OH, the three triplets and one singlet of the model convert into four doublets, of which two are $^2\Pi_{1/2}$ and two are $^2\Pi_{3/2}$ states. The dynamics is implemented using the diabatic Hamiltonian of Hoffmann and Schatz.[16] In this representation, the two of the three triplet surfaces are taken to be the $^3A''$ surface (both identical in the diabatic representation) of Ref. 14, and the other triplet is the $^3A'$ surface from the same paper. The singlet surface is the $^1A'$ of Ref. 15. The surfaces are sketched in Fig. 1.

The wave-packet reaction probabilities on the diabatic surfaces are computed as sums over trajectories in the product region,

$$P_i^d = \sum_k |\chi_i(\mathbf{x}_k)|^2 w_k h(\mathbf{x}_k),$$

where the index k labels trajectories and i labels the surfaces. The function $h(\mathbf{x})$ defines the product region

$$h(\mathbf{x}) = \tfrac{1}{4}(1-\tanh[\kappa(d_{\mathrm{OH}}-\bar{d}_{\mathrm{OH}})])(1+\tanh[\kappa(d_{\mathrm{HH}}-\bar{d}_{\mathrm{HH}})]), \quad (24)$$

where the distances d_{HH} and d_{OH} are the bond lengths between the hydrogens and between the oxygen and a selected hydrogen, respectively. The parameter values are $\bar{d}_{\mathrm{OH}}=3$, $\bar{d}_{\mathrm{HH}}=6$, and $\kappa=4$. Surfaces correlating with $^3P_0$ and $^1D_2$ states of oxygen are modified using the function $h(\mathbf{x})$ of Eq. (24), $\tilde{V}_{3(4)}=(1-h(\mathbf{x}))V_{3(4)}+h(\mathbf{x})V_1$, to ensure numerical equivalence of all four surfaces in the product region. The first and third surfaces correlate with the $^3P_2$ and $^3P_0$ states of oxygen. They remain coupled in the product region, correlating with the $^2\Pi_{3/2}$ and $^2\Pi_{1/2}$ states of OH. The other two surfaces correlate with the $^3P_1$ and $^1D_2$ states of oxygen and are also coupled in the product region, correlating with $^2\Pi_{3/2}$ and $^2\Pi_{1/2}$ states of OH.

Taking the sign of the asymptotic couplings into account, the adiabatic wave functions of the lower doubly degenerate state, $^2\Pi_{3/2}$, are

$$\psi_1^a = \frac{\psi_1-\psi_3}{\sqrt{2}}, \quad \psi_2^a = \frac{\psi_2+\psi_4}{\sqrt{2}}, \quad (25)$$

and of the higher doubly degenerate state, $^2\Pi_{1/2}$, are

$$\psi_3^a = \frac{\psi_1+\psi_3}{\sqrt{2}}, \quad \psi_4^a = \frac{\psi_2-\psi_4}{\sqrt{2}}. \quad (26)$$

The propagation is terminated once the adiabatic probabilities,

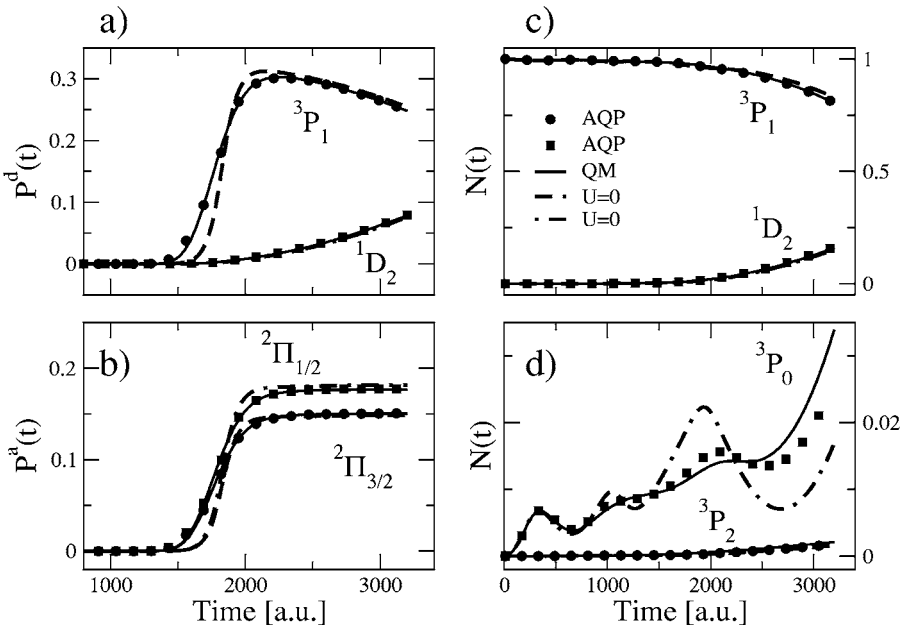

FIG. 2. Dynamics of the wave packet initialized on $^3P_1$ with $p_0=16$ (solid lines show QM results): (a) Reaction probabilities on the diabatic surfaces correlating with $^3P_1$ (AQP/classical results are shown with circles/dash) and with $^1D_2$ (AQP/classical results are shown as squares/dot dash); (b) reaction probabilities on the adiabatic surfaces correlating with $^2\Pi_{3/2}$ (AQP/classical results are shown with circles/dash) and with $^2\Pi_{1/2}$ (AQP/classical results are shown as squares/dot-dash); (c) population on $^3P_1$ and $^1D_2$ [legend is the same as in (a)]; (d) population on $^3P_2$ (AQP/classical results are shown with circles/dash) and with $^3P_0$ (AQP/classical results are shown as squares/dot dash).

$$P_i^a = \sum_k |\chi_i^a(\mathbf{x}_k)|^2 w_k h(\mathbf{x}_k),$$

reach constant values. The initial wave packet is a direct product of a Gaussian in the translational coordinate and the ground state of the ith PES in the internal degrees of freedom

$$\psi_i(x,y,\theta,0) = \left(\frac{2\alpha}{\pi}\right)^{1/4} \exp(-\alpha(x-x_0)^2 + ip_0(x-x_0))\xi(y). \quad (27)$$

Wave packets initially in the triplet state, $i=1,2,3$, were considered. The remaining wavefunction components are zeros: $\psi_j=0, j\neq i$. The parameters of the translational wave packet are $\alpha=4$, $x_0=7$, and $p_0=\{8,10,12,14,16,18\}$. The vibrational eigenstate is taken as the ground state of a Morse potential,[41] V_m, approximating the H_2 interaction,

$$V_m = D(1-\zeta)^2, \quad \zeta(y) = \exp[-z(y-y_m)],$$

$$D = 0.169, \quad z = 1.06, \quad y_m = 1.41. \quad (28)$$

The vibrational initial wave function is

$$\xi(y) = (2\lambda\zeta k)^{\lambda-1/2} \exp(-\lambda\zeta), \quad \lambda = \sqrt{2Dm}/z, \quad (29)$$

where k is the normalization constant, $k=8.6286\times10^{-2}$.

The calculations were performed using 2000–4000 trajectories with the Sobol pseudo-random sampling of the initial positions in three dimensions.[42] The deviates were uniform in $\cos\theta$ and normal (Gaussian) in the distances. Therefore, the trajectory weights are equal to the ratio of the density $|\xi(y)|^2$ to its Gaussian approximation divided by the number of trajectories. The initial momenta are $\mathbf{p}=(p_0,0,0)$. The initial action function is $S(x,y,\theta,0)=p_0(x-x_0)$. As established in single surface calculations[18] the θ component of the nonclassical momentum, r_θ, is small compared to the radial components and, therefore, it was set to zero in all trajectory calculations. The classical results are obtained by setting the quantum potential to zero, $U=0$. In this regime trajectories can be propagated independently of each other under the influence of V_d, but their initial conditions are the same as for the quantum trajectories. Approximation to the radial components r_x, r_y within the linear basis $\eta=\{1, x-x_0, y-y_m\}$ results in the linearized quantum force (LQF) approximation which is exact for Gaussian wave packets. In order to improve the description of H_2 asymptotically we add the exponential function $\zeta(y)$ given by Eq. (28) to the linear basis η. Such a basis gives an exact description of the Morse potential eigenstates.[18] If optimized coefficients of $\zeta(y)$ in the expansion of r_x or r_y were found negative, then their values were set to zero: negative values do not correspond to a normalizable density and can produce unphysically large quantum force.

The classical and LQF calculations were performed using 2000 trajectories with the exception of the lowest-energy calculation where twice as many trajectories were used due to small reaction probability. Calculations with the extended basis η were performed using 4000 trajectories because higher accuracy of the overlaps and moments of the basis functions is required in this case. The time step was taken $dt=2.5$ and $dt=3.0$ and the propagation time from 3200 to 4200 a.u. depending on the translational momentum p_0. Computation of PESs and couplings was the most expensive part of the trajectory calculation and the ability to make longer time steps was important. We used a second-order expansion in dt to propagate the complex functions χ_i according to Eq. (20).

A comparison is made with the time-dependent quantum calculations performed using the split-operator method[43,44] implemented within the grid representation for x and y and the discrete variable representation[45] for θ. The grid is 256×256 points with a spacing of 0.08 and the number of the discrete variable representation (DVR) points is 60. The action of the potential part of the Hamiltonian,

$$\exp(-i\mathbf{V}dt)\boldsymbol{\psi} = \tilde{\mathbf{V}}\boldsymbol{\psi}, \quad \tilde{\mathbf{V}} = \mathbf{M}\Lambda\mathbf{M}^T, \quad (30)$$

is accomplished by diagonalizing the potential matrix. The matrix $\mathbf{M}$ consists of the eigenvectors of $\mathbf{V}$. The elements of

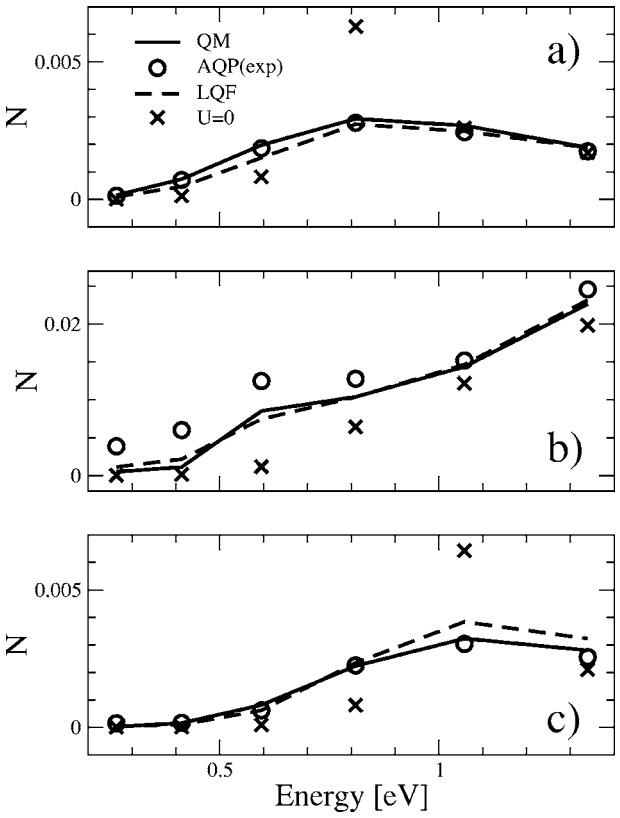

FIG. 3. Population N on the $^1D_2$ surface for the wave packets initialized on (a) $^3P_2$, (b) $^3P_1$, and (c) $^3P_0$ surfaces as a function of the initial translational energy. Quantum (solid line), AQP with (circles) and without (dash) the exponent and classical (crosses) results are shown on all panels.

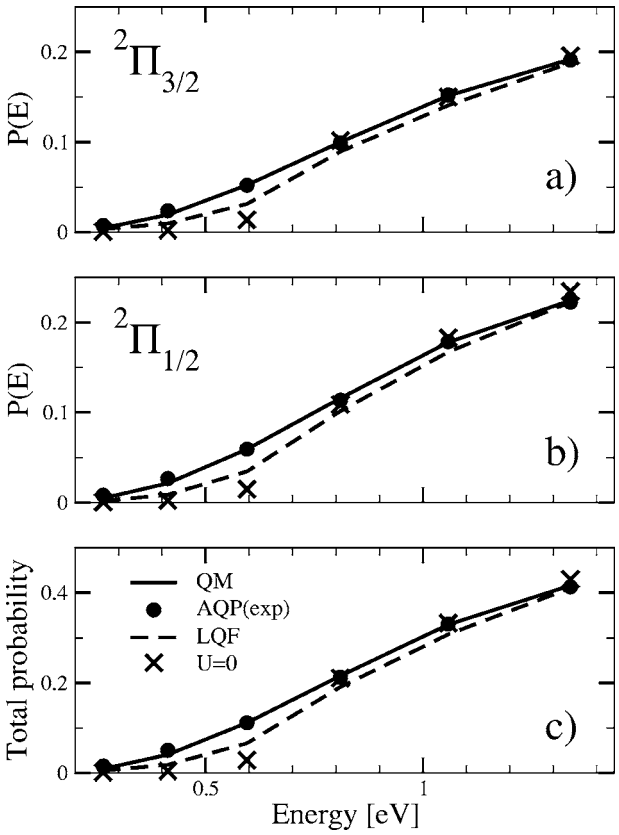

FIG. 4. Reaction probabilities for the wave packet initialized on $^3P_1$ obtained using QM (solid line), AQP with (circles) and without (dash) exponential function, and classical (crosses) propagation methods: (a) Probability of the reaction to $^2\Pi_{3/2}$; (b) probability of the reaction to $^2\Pi_{1/2}$; (c) reaction probability summed over all electronic states.

the diagonal matrix Λ are functions of the eigenvalues λ_i of the potential matrix $\mathbf{V}$, $\Lambda_{ii}=\exp(-i\lambda_i dt)$. The matrices $\tilde{\mathbf{V}}$ were stored for each grid point. Approximate propagation of the function $\boldsymbol{\chi}$ given by Eq. (20) can be accomplished according to Eq. (30) as well, but we found that determination of the eigenvectors of $\mathbf{V}$ for each trajectory at every time step was expensive compared to the second-order expansion in dt and gave essentially the same accuracy.

B. Results

We find that for the given system the coupling of the triplet surfaces to the singlet has essentially no effect on the wave-packet dynamics, and affects only the splitting between the doublet states of the product. The time-dependent reaction probabilities and populations of a wave packet initialized on the second surface ($^3P_1$) with translational momentum $p_0=16$ are shown in Fig. 2. The diabatic probabilities of the surfaces 2 and 4 obtained using QM and approximate propagation are shown on Fig. 2(a). The probabilities begin to oscillate between these two diabatic surfaces as the reactive part of the wave packet evolves in the product channel. The reaction probability on the other two diabatic surfaces is negligible. The adiabatic probabilities shown in Fig. 2(b) approach constant values after approximately $t=2300$. Panels (c) and (d) show the population of the diabatic surfaces as functions of time. Note that population on the surfaces 1 and 3 remain below a few percent at all times. The AQP result with the exponential basis function are in good agreement with the QM results. For this high-energy wave packet the classical results also agree quite well with the QM results at long times, though the wave-packet density is overly localized.

Figure 3 gives a qualitative picture of the triplet-singlet coupling on dynamics. We have observed that the singlet populations for the wave packets initialized on surface 1 exhibit maxima before reaching the product asymptotic region at approximately $t=\{2500,2400,2300,2000,1900,1900\}$ for the initial translational momenta $p_0=\{8,10,12,14,16,18\}$, respectively. The population on $^1A'$ at these times for the wave packets initialized on all triplet surfaces are shown in the figure. For the surfaces $^3P_2$ and $^3P_0$ the populations are below 0.003 and the semiclassical results are in good agreement with the QM ones. For the $^3P_1$ surface, the population of $^1A'$ is below 0.025. Classical ($U=0$) propagation gives a qualitative description of the nonadiabatic effect with the discrepancy coming from quantum corrections on the single surface dynamics.

Figure 4 shows adiabatic [$^2\Pi_{3/2}$ electronic state in Fig. 4(a) and $^2\Pi_{1/2}$ state in Fig. 4(b)] and total [summed over the electronic states in Fig. 4(c)] reaction probabilities as functions of the initial translational energy for the wave packet initialized on the $^3P_1$ surface. The overall quality of the description is the same as for the single surface dynamics reported in Ref. 18. The classical results underestimate probabilities at energies below the barrier to the reaction. The

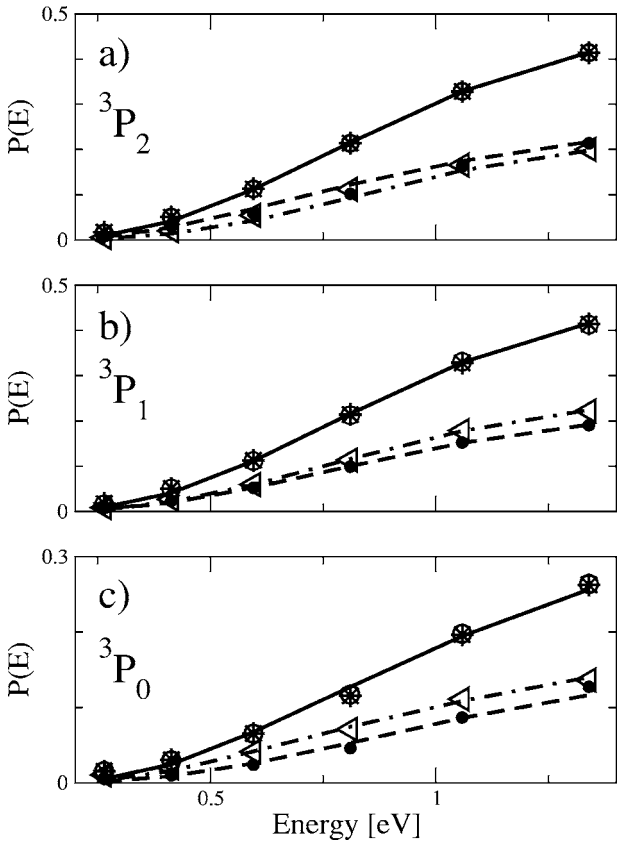

FIG. 5. Wave-packet reaction probabilities for the wave packet initialized on (a) $^3P_2$, (b) $^3P_1$, and (c) $^3P_0$ surfaces as functions of energy. Probabilities of reaction to $^2\Pi_{3/2}$ are shown with dash (QM) and filled circles (AQP). Probabilities of reaction to $^2\Pi_{1/2}$ are shown with dot dash (QM) and triangles (AQP). Their sum is shown with the solid line (QM) and open circles. Stars indicate the single surface AQP results.

AQP obtained with the linear basis partially corrects for this deficiency. Use of the exponential basis function gives accurate probabilities. Since the total, adiabatic, and single surface probabilities show similar agreement with the quantum results, approximations made to the time evolution of the population functions χ_i are consistent with approximate trajectory dynamics for this system.

The total probabilities and the probabilities of reaction to the $^2\Pi_{3/2}$ and $^2\Pi_{1/2}$ states for the wave packets initialized on the $^3P_{2,1,0}$ surfaces are shown in Fig. 5. The QM and AQP with the exponential basis function are shown. The single surface AQP results are in close agreement with the total probabilities for the nonadiabatic problem. The semiclassical splittings between the two doublet states are underestimated compared to the QM result for the wave packet started in the $^3P_2$ state. The splittings for the states $^3P_1$ and $^3P_0$ are in good agreement with the QM results.

IV. CONCLUSIONS

Nonadiabatic effects in the $O(^3P_{2,1,0}, ^1D_2)+H_2$ system were studied using the mixed coordinate space/polar representation of the wave function. The polar part describing overall wave function dynamics was propagated semiclassically and represented in terms of quantum trajectories evolving under the combined influence of the effective classical and approximate quantum potentials. The effective classical potential was defined as a linear combination of the four diabatic surfaces weighted according to their populations. The population functions were represented as prefactors computed approximately for each trajectory. Representation of the nonclassical component of the momentum operator (acting on the polar part and defining the AQP) in terms of a small basis is the only approximation in the quantum trajectory propagation. Omission of the population functions derivatives that were minimized by the choice of the effective potential is the only approximation in the population function evolution.

We find that for this direct dynamics reaction the effects of diabatic coupling and single surface quantum effects on dynamics can be treated separately. Population of the singlet state in the interaction region of PESs is found to be small (well below 2% in most cases). Classical results reproduce the coupling effect fairly well, especially at high energies where quasiclassical TSH calculations indicated enhanced reaction probabilities (compared to the single surface probabilities).[10] Introduction of the linearized quantum force corrects single surface quantum effects in the dynamics and improves agreement with the QM probabilities. Inclusion of the exponential function into the basis gives accurate reaction probabilities. Overall, the intersystem crossing effect on the reaction probability from the ground rovibrational state in $O(^3P,^1D)+H_2 \rightarrow OH+H$ is found to be negligible in all of our trajectory-based and quantum calculations which is consistent with the recent quantum wave-packet study of the reaction cross section by Chu *et al.*[13]

[1] L. J. Butler, Annu. Rev. Phys. Chem. **49**, 125 (1998).
[2] L. Sun, K. Song, and W. L. Hase, Science **296**, 875 (2002).
[3] S. C. Ammal, H. Yamataka, M. Aida, and M. Dupuis, Science **299**, 1555 (2003).
[4] J. C. Tully, J. Chem. Phys. **93**, 1061 (1990).
[5] J. C. Tully, Faraday Discuss. **110**, 407 (1998).
[6] Z. Qu, H. Zhu, S. Y. Grebenshchikov, and R. Schinke, J. Chem. Phys. **122**, 191102 (2005).
[7] E. Martinez-Nunez, S. Vazquez, G. Granucci, M. Persico, and C. M. Estevez, Chem. Phys. Lett. **412**, 35 (2005).
[8] B. Maiti and G. C. Schatz, J. Chem. Phys. **119**, 12360 (2003).
[9] D. C. Robie, S. Arepalli, N. Presser, T. Kitsopoulos, and R. J. Gordon, J. Chem. Phys. **92**, 7382 (1990).
[10] D. J. Garton, T. K. Minton, B. Maiti, D. Troya, and G. C. Schatz, J. Chem. Phys. **118**, 1585 (2003).
[11] M. Braunstein, S. Adler-Golden, B. Maiti, and G. C. Schatz, J. Chem. Phys. **121**, 4316 (2004).
[12] N. Balakrishnan, J. Chem. Phys. **119**, 195 (2003).
[13] T.-S. Chu, X. Zhang, and K.-L. Han, J. Chem. Phys. **122**, 213201 (2005).
[14] S. Rogers, D. Wang, A. Kuppermann, and S. Walch, J. Phys. Chem. A **104**, 2308 (2000).
[15] A. J. Dobbyn and P. J. Knowles, Faraday Discuss. **110**, 247 (1998).
[16] M. R. Hoffmann and G. C. Schatz, J. Chem. Phys. **113**, 9456 (2000).
[17] S. Garashchuk and V. A. Rassolov, Chem. Phys. Lett. **376**, 358 (2003).
[18] V. A. Rassolov, S. Garashchuk, and G. C. Schatz, J. Phys. Chem. A **110**, 5330 (2006).
[19] V. A. Rassolov and S. Garashchuk, Phys. Rev. A **71**, 032511 (2005).
[20] S. Garashchuk, V. A. Rassolov, and G. C. Schatz, J. Chem. Phys. **123**, 174108 (2005).
[21] D. Bohm, Phys. Rev. **85**, 166 (1952).
[22] S. Garashchuk and V. A. Rassolov, J. Chem. Phys. **120**, 1181 (2004).
[23] V. A. Rassolov and S. Garashchuk, J. Chem. Phys. **120**, 6815 (2004).
[24] S. Garashchuk and V. A. Rassolov, J. Chem. Phys. **121**, 8711 (2004).
[25] C. L. Lopreore and R. E. Wyatt, Phys. Rev. Lett. **82**, 5190 (1999).
[26] E. R. Bittner, J. Chem. Phys. **112**, 9703 (2000).

[27] R. E. Wyatt and E. R. Bittner, J. Chem. Phys. **113**, 8898 (2000).
[28] B. K. Kendrick, J. Chem. Phys. **119**, 5805 (2003).
[29] D. Babyuk and R. E. Wyatt, J. Chem. Phys. **121**, 9230 (2004).
[30] B. Poirier, J. Chem. Phys. **121**, 4501 (2004).
[31] J. Liu and N. Makri, J. Phys. Chem. A **108**, 5408 (2004).
[32] I. Burghardt and L. S. Cederbaum, J. Chem. Phys. **115**, 10303 (2001).
[33] I. Burghardt and L. S. Cederbaum, J. Chem. Phys. **115**, 10312 (2001).
[34] I. Burghardt and K. B. Moller, J. Chem. Phys. **117**, 7409 (2002).
[35] J. B. Maddox and E. R. Bittner, J. Phys. Chem. B **106**, 7981 (2002).
[36] E. R. Bittner, J. B. Maddox, and I. Burghardt, Int. J. Quantum Chem. **89**, 313 (2002).
[37] A. Donoso and C. C. Martens, Phys. Rev. Lett. **87**, 223202 (2001).
[38] C. J. Trahan and R. E. Wyatt, J. Chem. Phys. **119**, 7017 (2003).
[39] B. K. Kendrick, J. Chem. Phys. **121**, 2471 (2004).
[40] R. E. Wyatt and K. Na, Phys. Rev. E **65**, 016702 (2002).
[41] P. M. Morse, Phys. Rev. **34**, 57 (1929).
[42] W. Press, B. Flannery, S. Teukolsky, and W. Vetterling, *Numerical Recipes: The Art of Scientific Computing* 2nd ed. (Cambridge University Press, Cambridge, 1992).
[43] C. Leforestier, R. H. Bisselling, C. Cerjan *et al.*, J. Comput. Phys. **94**, 59 (1991).
[44] M. D. Feit, J. A. Fleck, and A. Steiger, J. Comput. Phys. **47**, 412 (1982).
[45] J. C. Light, I. P. Hamilton, and J. V. Lill, J. Chem. Phys. **82**, 1400 (1985).